Implementation of the Deutsch–Jozsa algorithm on an ion-trap quantum computer

Stephan Gulde*, Mark Riebe*, Gavin P. T. Lancaster*, Christoph Becher*, Jürgen Eschner*, Hartmut Häffner*, Ferdinand Schmidt-Kaler*, Isaac L. Chuang*† & Rainer Blatt*

** Institut für Experimentalphysik, Universität Innsbruck, Technikerstraße 25, A-6020 Innsbruck, Austria*
† MIT Media Laboratory, Cambridge, Massachusetts 02139, USA

Determining classically whether a coin is fair (head on one side, tail on the other) or fake (heads or tails on both sides) requires an examination of each side. However, the analogous quantum procedure (the Deutsch–Jozsa algorithm[1,2]) requires just one examination step. The Deutsch–Jozsa algorithm has been realized experimentally using bulk nuclear magnetic resonance techniques[3,4], employing nuclear spins as quantum bits (qubits). In contrast, the ion trap processor utilises[5] motional and electronic quantum states of individual atoms as qubits, and in principle is easier to scale to many qubits. Experimental advances in the latter area include the realization of a two-qubit quantum gate[6], the entanglement of four ions[7], quantum state engineering[8] and entanglement-enhanced phase estimation[9]. Here we exploit techniques[10,11] developed for nuclear magnetic resonance to implement the Deutsch–Jozsa algorithm on an ion-trap quantum processor, using as qubits the electronic and motional states of a single calcium ion. Our ion-based implementation of a full quantum algorithm serves to demonstrate experimental procedures with the quality and precision required for complex computations, confirming the potential of trapped ions for quantum computation.

Laser-cooled trapped ions are ideally suited to the investigation and implementation of quantum information processing[12] because they exhibit these properties: (1) localization of the single particle to less than a few tens of nanometres[13–15]; (2) control of the motional state down to the zero point of the trapping potential[8,16]; (3) a high degree of isolation from the environment and thus a very long time available for manipulations of their quantum state[17]; and (4) the ability to detect the ion's quantum state with high precision by the electron shelving technique[18]. The same properties make single trapped ions well suited for storing quantum information in long-lived internal states[19].

In our experiment we implement the Deutsch–Jozsa algorithm on a quantum processor based on a single trapped $^{40}Ca^{+}$ ion which is driven by laser pulses. A compensation technique for frequency shifts allows us to achieve the required control over the optical phases of the pulses[20]. Following a recent proposal[10], we also successfully combine ion-trap techniques for quantum state manipulation with the method of composite pulses[11] adopted from NMR technology. Thus we achieve complete control over the ion's motional and electronic state. The implementation of a quantum algorithm on an ion-trap processor, which we demonstrate here, serves as a test of the suitability of these techniques, particularly in view of their scalability towards a larger number of qubits.

To illustrate the Deutsch–Jozsa algorithm, we represent the four possible coins by four functions f that map one input bit ($a = 0,1$ standing for 'which side of the coin') onto one output bit ($f(a) = 0,1$ standing for 'head or tail'). These functions can be divided into two constant functions $f_1(a) = 0$, $f_2(a) = 1$, representing the fake coins, and two balanced functions $f_3(a) = a$, $f_4(a) =$ NOT a, which stand for the fair coins (see Table 1). An unknown function is characterized as constant or balanced by evaluating $f(0) \oplus f(1)$ which yields 0 (or 1) for a constant (or balanced) function ($\oplus$ denotes addition modulo 2). This evaluation classically requires two function calls, whereas the Deutsch–Jozsa quantum algorithm allows us to obtain the desired information with a single evaluation of the unknown f. The circuit diagram shown in Fig. 1 describes the implementation of the Deutsch–Jozsa algorithm with basic quantum operations[21]. The two qubits required for the Deutsch–Jozsa algorithm are encoded in the electronic state and in the phonon (vibrational quantum) number of the axial vibration mode of the single trapped ion (see Fig. 2). Qubit operations are realized by applying laser pulses on the 'carrier' or the 'blue sideband' of the electronic quadrupole transition as described in the Methods.

In general, a quantum algorithm is implemented by a sequence of such pulses on the carrier and sideband, but two major sources of error have to be overcome. First, as the simplest algorithms already require several pulses, we need to control precisely the relative optical phases of these pulses or, at least, to keep track of them such that the required pulse sequences lead to the desired operations. In particular, this requires the precise investigation and subsequent compensation of all phases introduced by the light shifts of the exciting laser beams. These light shifts arise as we have to drive

Table 1 **Truth table for the four possible functions**

	Constant functions		Balanced functions	
	Case 1	Case 2	Case 3	Case 4
$f(0)$	0	1	0	1
$f(1)$	0	1	1	0
$w \oplus f(a)$	ID	NOT	CNOT	Z-CNOT

The third line is the effect of the logic function U_{f_n} on the qubit w: ID denotes the identity, CNOT is a controlled NOT operation, Z-CNOT is a zero controlled NOT, and the control bit in cases 3 and 4 is the input bit a.

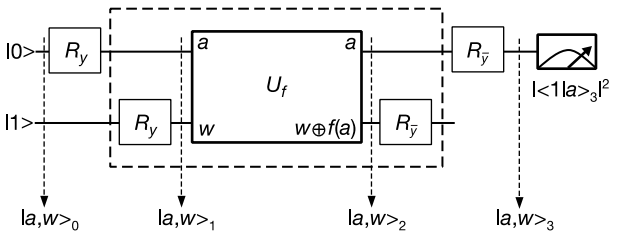

Figure 1 Quantum circuit for implementing the Deutsch–Jozsa algorithm with basic quantum operations. The upper line shows the input qubit $|a\rangle$ ('which side of the coin' information), the lower line an auxiliary working qubit $|w\rangle$ (corresponding to the channel on which the answer is provided). The rotations R_y (see Methods for details) create superpositions $|a\rangle_1 = (|0\rangle + |1\rangle)/\sqrt{2}$ and $|w\rangle_1 = (|0\rangle - |1\rangle)/\sqrt{2}$ from the inputs $|a\rangle_0 = |0\rangle$ and $|w\rangle_0 = |1\rangle$. The box U_{f_n} represents a unitary operation specific to each of the functions f_n, which applies f_n to a and adds the result to w modulo 2. Table 1 lists the logic operations required for transforming $|w\rangle$ into $|w \oplus f_n(a)\rangle$. The output of the box is $|a, w\rangle_2 = (|0, w_{\text{in}} \oplus f_n(0)\rangle + |1, w_{\text{in}} \oplus f_n(1)\rangle)/\sqrt{2}$. Up to an overall sign $|w\rangle$ is left unchanged, but the positive superposition $(|0\rangle + |1\rangle)/\sqrt{2}$ on $|a\rangle$ is transformed into a negative superposition $|a\rangle_2 = (|0\rangle - |1\rangle)/\sqrt{2}$ if f is balanced; otherwise it is unchanged. After the final rotations $R_{\bar{y}}$, a measurement on $|a\rangle$ is performed with result $|a\rangle_3 =$ either $|0\rangle$ or $|1\rangle$. Because of the sign change in $|a\rangle_2$ if f is balanced, $|\langle 1 \mid a\rangle_3|^2 = f_n(0) \oplus f_n(1)$, that is, $|a\rangle_3$ yields the desired information whether the function f_n is balanced or constant. The working qubit w resumes its initial value $|w\rangle_3 = |w\rangle_0 = |1\rangle$.

sideband transitions (which couple much more weakly than carrier transitions) with high laser intensity. We cancel the unwanted light shifts with an additional off-resonant laser field, inducing a light shift of equal strength but opposite sign[20].

Second, a peculiarity of encoding a qubit within the ion's motional state is that we must ensure that the system does not leave the computational subspace $\{|S,0_z\rangle, |D,0_z\rangle, |S,1_z\rangle, |D,1_z\rangle\}$ (for notation, see Methods). The main problem here is that owing to the degenerate spectrum of a harmonic oscillator, sideband pulses work simultaneously on all levels. Therefore any population in $|S,1_z\rangle$ prior to a blue sideband pulse will leave the computational subspace. To avoid this, we use composite pulses, that is, a sequence of carrier and/or sideband pulses that—up to an overall phase—constrain the system to the subspace[10]. We adopted this method from NMR technology[11]. The translation of the Deutsch—Jozsa algorithm into composite pulses acting on the two qubits is described in the Methods.

For our experiments we load Ca ions into a linear Paul trap with axial frequency $\omega_z \approx 2\pi \times 1.7\,\mathrm{MHz}$. Figure 2 shows the relevant optical transitions used for laser cooling, state preparation and detection. Each experimental cycle starts with Doppler cooling for 2 ms on the $S_{1/2} \rightarrow P_{1/2}$ transition yielding average vibrational quantum numbers $\bar{n}_z \approx 20$. Further cooling of the axial motion to a ground state occupation of more than 99% is achieved by about 12 ms of sideband cooling[8]. To initalize the quantum processor in $|01\rangle = |S,0_z\rangle$, we optically pump the ion to the $S_{1/2}$ $(m = -1/2)$ state. Manipulations of both qubits are achieved by pulses from a stabilized titanium–sapphire laser (linewidth < 100 Hz, relative intensity noise $< 0.02_{\mathrm{r.m.s.}}$) emitting at the $S_{1/2} \leftrightarrow D_{5/2}$ transition wavelength near 729 nm. In order to switch between R and R^+ rotations we shift the laser frequency with an acousto-optical modulator. The phase of the light field is switched via the phase of the radio frequency driving the acousto-optical modulator with an inaccuracy of less than 0.06 rad. Using the electron shelving technique[8] we detect the ion's electronic state ($S_{1/2}$ or $D_{5/2}$) with a fidelity of 99.9% within a detection time of 3 ms.

We measure the fidelity of the implemented algorithm by repeating several thousand times the experimental sequence of cooling, initialization of both qubits, laser pulses for the algorithm and final measurement. Table 2 displays the achieved results. For cases 1, 3 and 4, the fidelity of identifying the function's class with a single measurement exceeds 97%; for case 2, it is above 90%. Note

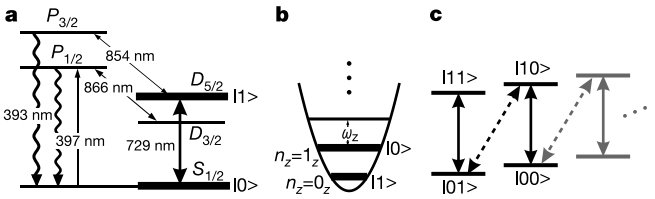

Figure 2 Quantum mechanical energy levels relevant for the ion-trap quantum computer. **a**, Ca^+ level scheme. The upper and lower electronic states $S_{1/2}$ $(m = -1/2)$ and $D_{5/2}$ $(m = -1/2)$ of the narrow quadrupole transition ($\tau_D \approx 1$ s) at 729 nm serve to implement one of the qubits, $|a\rangle$. Coherent radiation of a titanium–sapphire laser at 729 nm drives the qubit transition. Lasers at 397 nm, 866 nm and 854 nm are used for the excitation of resonance fluorescence, for Doppler cooling, and optical pumping. The laser system is described in detail elsewhere[19]. **b**, The lowest two number states, $n_z = 0_z, 1_z$, of the axial vibrational motion in the trap form the other qubit, $|w\rangle$. **c**, The combination of electronic states and energy eigenstates of the harmonic oscillator potential span the computational subspace. Numbers in ket notation denote the quantum logical values assigned to the respective states. Solid lines show carrier transitions; dashed lines show blue sideband transitions.

Table 2 **Expected and measured results of the complete Deutsch–Jozsa algorithm**

	Constant		Balanced	
	Case 1	Case 2	Case 3	Case 4
Expected $\|\langle 1 \mid a\rangle\|^2$	0	0	1	1
Measured $\|\langle 1 \mid a\rangle\|^2$	0.019(6)	0.087(6)	0.975(4)	0.975(2)
Expected $\|\langle 1 \mid w\rangle\|^2$	1	1	1	1
Measured $\|\langle 1 \mid w\rangle\|^2$	–	0.90(1)	0.931(9)	0.986(4)

The numbers in brackets are statistical 1σ uncertainties.

that to decide whether the function is constant or balanced, only $|\langle 1 \mid a\rangle_3|^2$ at the end of the algorithm needs to be measured. We also verified that the working qubit $|w\rangle$ is reset to its initial value by reading out the phonon number through a measurement of the Rabi frequency of the blue sideband transition[8,16].

The measured output of the algorithm shown in Table 2 slightly deviates from the ideal result. We identified the major sources for this infidelity and attribute it mainly to decoherence of the laser-atom phase, in particular caused by ambient magnetic field fluctuations[22]. Furthermore, in the implementation of case 2, which requires the most complex pulse sequence, we used higher laser power of the sideband transitions in order to speed up the algorithm and thus reduce the sensitivity to phase decoherence. This in turn caused off-resonant carrier excitation which limited the obtainable fidelity.

A major advantage of our state detection technique is the ability to follow the evolution of $|\langle 1 \mid a\rangle|^2$ during the quantum algorithm. For this, we truncate the pulse sequence at a certain time t and reveal $|\langle 1 \mid a(t)\rangle|^2$ by measuring the probability of finding the ion in the $D_{5/2}$ state. In Fig. 3 we display this probability as a function of time for all four cases. The data agree very well with the calculated ideal

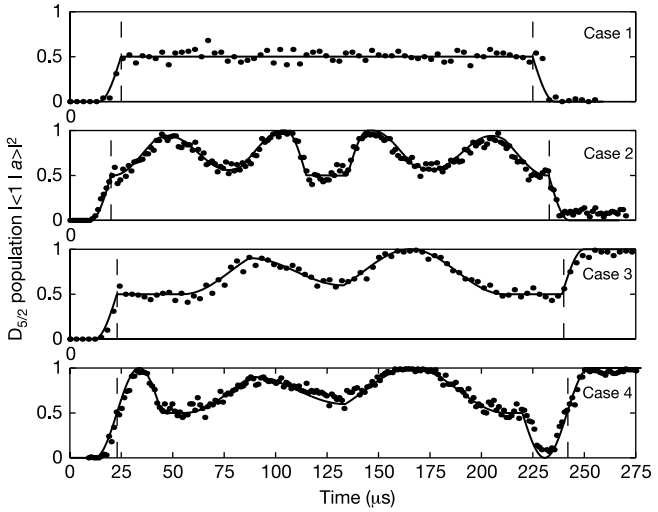

Figure 3 Time evolution of $|\langle 1 \mid a\rangle|^2$. Points are the probabilities, each inferred from 100 measurements, the line shows the ideal evolution. No parameters were adjusted to fit the data. The implementation of the functions $R_{\bar{y}_w} U_{f_n} R_{y_w}$ takes place between the dashed lines. An initial R_{y_a} and a final $R_{\bar{y}_a}$ rotation on $|a\rangle$, implemented by carrier pulses, complete the algorithm. Taking case 3 as an the example, R_{y_a} lasts from 12 μs to 22 μs. Then $R_{\bar{y}_w} U_{f_n} R_{y_w}$ on $|a,w\rangle$ is implemented from 54 μs to 212 μs with the laser tuned to the blue sideband. The laser phase is switched at 87, 133 and 166 μs according to Table 3. The final $R_{\bar{y}_a}$ pulse is applied from 240 to 250 μs.

Table 3 **Implementations of $R_{\tilde{y}_w} U_{f_n} R_{y_w}$**

	Logic	Laser pulses
f_1	$R_{\tilde{y}_w} R_{y_w}$	No pulses
f_2	$R_{\tilde{y}_w}$ SWAP^{-1} NOT$_a$ SWAP R_{y_w}	$R^+\left(\frac{\pi}{\sqrt{2}},0\right)R^+\left(\frac{2\pi}{\sqrt{2}},\varphi_{\mathrm{SWAP}}\right)R^+\left(\frac{\pi}{\sqrt{2}},0\right)$ $R\left(\frac{\pi}{2},0\right)R\left(\pi,\frac{\pi}{2}\right)R\left(\frac{\pi}{2},\pi\right)$ $R^+\left(\frac{\pi}{\sqrt{2}},\pi\right)R^+\left(\frac{2\pi}{\sqrt{2}},\pi+\varphi_{\mathrm{SWAP}}\right)R^+\left(\frac{\pi}{\sqrt{2}},\pi\right)$
f_3	$R_{\tilde{y}_w}$ CNOT R_{y_w}	$R^+\left(\frac{\pi}{\sqrt{2}},0\right)R^+\left(\pi,\frac{\pi}{2}\right)R^+\left(\frac{\pi}{\sqrt{2}},0\right)R^+\left(\pi,\frac{\pi}{2}\right)$
f_4	$R_{\tilde{y}_w}$ Z-CNOT R_{y_w}	$R(\pi,0)R^+\left(\frac{\pi}{\sqrt{2}},0\right)R^+\left(\pi,\frac{\pi}{2}\right)R^+\left(\frac{\pi}{\sqrt{2}},0\right)R^+\left(\pi,\frac{\pi}{2}\right)R(\pi,0)$

The rotation angle for $R^+(\theta,\varphi)$ is given for the $|10\rangle \rightarrow |01\rangle$ transition. θ and φ denote the pulse duration and phase, respectively. $\varphi_{\mathrm{SWAP}} = \arccos(\cot^2(\pi/\sqrt{2}))$, where the SWAP operation is explained in the Methods.

evolution (solid lines in Fig. 3, no fit parameters), demonstrating the high precision of the applied pulse sequence, especially the control over the optical phases.

The results demonstrate a high degree of control of all relevant experimental parameters, that is, laser frequency and intensity, optical phases, and trap frequency ω_z, over long pulse sequences. Therefore, the procedures presented here pave the way for implementing more complex algorithms and for scaling the system to multi-qubit operation. In particular, the light shift compensation technique demonstrated in this experiment can be directly transferred and advantageously applied to a several-qubit quantum processor. This technique will become increasingly important for scaling such a system because as the ion crystal becomes heavier, the higher laser intensities required to drive sideband transitions result in increased light shifts. Furthermore, by merging the composite pulse technique with our trapped-ion quantum computer we gain full access to all gate operations on the motional qubit. The employed composite-pulse phase gate also simplifies the Cirac–Zoller scheme[5] for a universal set of quantum gates, by dispensing with the auxiliary level transition. Thus our procedures become applicable to a wider choice of ion species including $^{43}Ca^+$, which offers a potentially much longer coherence time than $^{40}Ca^+$. □

Methods

Encoding of qubits and single-qubit rotations

The two qubits required for the Deutsch–Jozsa algorithm are encoded in the electronic quantum state ($S_{1/2}$ ($m=-1/2$) $\equiv |0\rangle \equiv |S\rangle$ and $D_{5/2}$ ($m=-1/2$) $\equiv |1\rangle \equiv |D\rangle$) and in the phonon number of the axial vibration mode of the single trapped ion ($n_z = 0_z \equiv |1\rangle$ and $n_z = 1_z \equiv |0\rangle$. Note the counterintuitive encoding of the vibrational mode, which simplifies the desired initial state preparation in $|01\rangle = |S,0_z\rangle$. The operations which modify the electronic qubit ('single-qubit rotations') are performed with laser pulses on the carrier ($|S,n_z\rangle \leftrightarrow |D,n_z\rangle$) transition, that is, no change of vibrational quantum number, laser on resonance. To connect the two qubits ('two-qubit rotations') the laser is detuned by $+\omega_z$ from the $|S\rangle \leftrightarrow |D\rangle$ resonance to the 'blue sideband' ($|S,n_z\rangle \leftrightarrow |D,n_z+1\rangle$) as indicated in Fig. 2. Qubit rotations can be written as unitary operations in the following way[12]:

Carrier rotations are given by

$$R(\theta,\phi) = \exp\left[i\frac{\theta}{2}(e^{i\phi}\sigma^+ + e^{-i\phi}\sigma^-)\right]$$

whereas transitions on the blue sideband are denoted as

$$R^+(\theta,\phi) = \exp\left[i\frac{\theta}{2}(e^{i\phi}\sigma^+ b^\dagger + e^{-i\phi}\sigma^- b)\right]$$

Here $\sigma^\pm$ are the atomic raising and lowering operators which act on the electronic quantum state of the ion, that is, the first qubit, by inducing transitions from the $|S\rangle$ to $|D\rangle$ state and vice versa (notation: $\sigma^+ = |D\rangle\langle S|$). The operators b and $b^\dagger$ stand for the annihilation and creation of a phonon at the trap frequency, that is, they work on the motional quantum state, the second qubit. The parameter θ depends on the strength and the duration of the applied pulse and ϕ is its phase, that is, the relative phase between the optical field and the atomic polarization. We use the definitions $R_y = R(\pi/2,0)$ and $R_{\tilde{y}} = R(\pi/2,\pi)$.

Translation of the Deutsch–Jozsa algorithm into composite pulses

The quantum circuit shown in Fig. 1 shows the quantum logic operations used for the implementation and Table 1 lists the logic functions corresponding to the unitary operations U_{f_n}. The R_y rotations on the electronic qubit $|a\rangle$ are carrier pulses. For efficient computation we combine the rotations $R_{\tilde{y}}, R_y$ on $|w\rangle$ and the manipulations for implementing U_{f_n} into an optimized pulse sequence, $R_{\tilde{y}_w} U_{f_n} R_{y_w}$ (dashed box in Fig. 1). As these operations act also on the motional state, we implement them with pulses on the carrier and the blue axial sideband. However, sideband pulses operate on both qubits simultaneously. Thus, for operations on $|w\rangle$ alone, we first swap the information from $|w\rangle$ into $|a\rangle$ with a sequence of three blue sideband pulses, then we rotate $|a\rangle$ as desired and swap back.

For a swap operation one might be tempted to use a single π-pulse on the blue sideband. However, applying this to the state $|00\rangle = |S,1_z\rangle$ leads to a population of states with two phonons outside the computational subspace. Therefore we use a composite pulse sequence consisting of three pulses, whose lengths are chosen such that starting from $|S,1_z\rangle$ the ion is rotated by π,2π and π, respectively. As a result the ion is rotated by 4π back to $|S,1_z\rangle$ independently of the pulses' relative phases. In addition, using the blue sideband ensures that $|11\rangle \equiv |D,0_z\rangle$ also stays unchanged as required for the swap operation.

The desired swap operation $|S,0_z\rangle \leftrightarrow |D,1_z\rangle$ is possible because compared to the $|S,1_z\rangle \leftrightarrow |D,2_z\rangle$ transition, the Rabi frequency for the $|S,0_z\rangle \leftrightarrow |D,1_z\rangle$ transition is smaller by $1/\sqrt{2}$ (refs 8, 16). So in this manifold the three pulses' lengths correspond to rotation angles of $\pi/\sqrt{2}, 2\pi/\sqrt{2}, \pi/\sqrt{2}$. It can be shown that choosing the laser-atom phase of the second pulse to be $\arccos(\cot^2(\pi/\sqrt{2})) = \pi 0.3033\ldots$ relative to the first and the third pulses, the populations of $|10\rangle = |D,1_z\rangle$ and $|01\rangle = |S,0_z\rangle$ are exchanged. This realises the desired swap. Table 3 (case 2) lists the complete pulse sequence for the implementation of $R_{\tilde{y}_w} U_{f_2} R_{y_w}$. Similar procedures are applied to realise the pulse sequences for cases 3 and 4. In these cases the rotations $R_{\tilde{y}_w}, R_{y_w}$ and the operations required for U_{f3}, U_{f4} can be combined in such a way that swap operations become unnecessary.

Received 21 October; accepted 27 November 2002; doi:10.1038/nature01336.

1. Deutsch, D. Quantum theory, the Church-Turing principle and the universal quantum computer. *Proc. R. Soc. Lond. A* **400,** 97–117 (1985).
2. Deutsch, D. & Jozsa, R. Rapid solution of problems by quantum computation. *Proc. R. Soc. Lond. A* **439,** 553–558 (1992).
3. Chuang, I. I., Vandersypen, I. M. K., Zhou, X., Leung, D. W. & Lloyd, S. Experimental realization of a quantum algorithm. *Nature* **393,** 143–146 (1998).
4. Jones, T. F. & Mosca, M. Implementation of a quantum algorithm to solve Deutsch's problem on a nuclear magnetic resonance quantum computer. *J. Chem. Phys.* **109,** 1648–1653 (1998).
5. Cirac, J. I. & Zoller, P. Quantum computations with cold trapped ions. *Phys. Rev. Lett.* **74,** 4091–4094 (1995).
6. Monroe, C., Meekhof, D. M., King, B. E., Itano, W. M. & Wineland, D. J. Demonstration of a fundamental quantum logic gate. *Phys. Rev. Lett.* **75,** 4714–4717 (1995).
7. Sackett, C. A. *et al.* Experimental entanglement of four particles. *Nature* **404,** 256–259 (2000).
8. Roos, Ch. *et al.* Quantum state engineering on an optical transition and decoherence in a Paul trap. *Phys. Rev. Lett.* **83,** 4713–4716 (1999).
9. Meyer, V. *et al.* Experimental demonstration of entanglement-enhanced rotation angle estimation using trapped ions. *Phys. Rev. Lett.* **86,** 5870–5873 (2001).
10. Childs, A. M. & Chuang, I. M. Universal quantum computation with two-level trapped ions. *Phys. Rev. A* **63,** 012306 (2001).
11. Levitt, M. H. Composite pulses (NMR spectroscopy). *Prog. Nucl. Magn. Reson. Spectrosc.* **18,** 61–122 (1986).
12. Šašura, M. & Bužek, V. Cold trapped ions as quantum information processors. *J. Mod. Opt.* **49,** 1593–1647 (2002).
13. Eschner, J., Raab, Ch., Schmidt-Kaler, F. & Blatt, R. Light interference from single atoms and their mirror images. *Nature* **413,** 495–498 (2001).
14. Guthöhrlein, G. R., Keller, M., Hayasaka, K., Lange, W. & Walther, H. A single ion as a nanoscopic probe of an optical field. *Nature* **414,** 49–51 (2001).
15. Mundt, A. B. *et al.* Coupling a single atomic quantum bit to a high finesse optical cavity. *Phys. Rev. Lett.* **89,** 103001 (2002).
16. Meekhof, D. M., Monroe, C., King, B. E., Itano, W. M. & Wineland, D. J. Generation of nonclassical motional states of a trapped atom. *Phys. Rev. Lett.* **76,** 1796–1799 (1996).
17. Monroe, C., Meekhof, D. M., King, B. E. & Wineland, D. J. A "Schrödinger Cat" superposition state of an atom. *Science* **272,** 1131–1136 (1996).
18. Dehmelt, H. Proposed $10^{14}\Delta\nu < \nu$ laser fluorescence spectroscopy on TI^+ mono-ion oscillator. *Bull. Am. Phys. Soc.* **20,** 60 (1975).
19. Nägerl, H. C. *et al.* Investigating a qubit candidate: Spectroscopy on the $S_{1/2}$ to $D_{5/2}$ transition of a trapped calcium ion in a linear Paul trap. *Phys. Rev. A* **61,** 023405 (2000).
20. Häffner, H. *et al.* Precision measurement and compensation of optical Stark shifts for an ion-trap quantum processor. Preprint available at ⟨http://arXiv.org/abs/physics/0212040⟩ (2002).
21. Nielsen, M. A. & Chuang, I. J. *Quantum Computation and Quantum Information* (Cambridge Univ. Press, Cambridge, 2000).
22. Schmidt-Kaler, F. *et al.* Coherence of qubits based on single Ca ions. Preprint available at ⟨http://arXiv.org/abs/quant-ph/0211059⟩ (2002).

Acknowledgements We gratefully acknowledge support by the European Commission (QSTRUCT, QI, QUEST and QUBITS networks), by the Austrian Science Fund (FWF), and by the Institut für Quanteninformation GmbH.

Competing interests statement The authors declare that they have no competing financial interests.

Correspondence and requests for materials should be addressed to F.S.-K. (e-mail: Ferdinand.Schmidt-Kaler@uibk.ac.at).